doi:10.1093/plphys/kiab249 PLANT PHYSIOLOGY 2021: 187: 174–186

Plant Physiology®

Research Article

The chloroplast ribosomal protein large subunit 1 interacts with viral polymerase and promotes virus infection

De-Jie Cheng ,[1] Xiao-Jie Xu,[1] Zhi-Yong Yan,[1] Carlos Kwesi Tettey ,[1] Le Fang,[1] Guang-Ling Yang,[1] Chao Geng ,[1] Yan-Ping Tian,[1,†] and Xiang-Dong Li ,[1,*]

1 Shandong Provincial Key Laboratory of Agricultural Microbiology, Laboratory of Plant Virology, Department of Plant Pathology, College of Plant Protection, Shandong Agricultural University, Tai'an, Shandong 27018, China

*Author for communication: xdongli@sdau.edu.cn
†Senior author.

D.C., Y.T., and X.L. designed the experiments; D.C., X.X., and Z.Y. performed the experiments; D.C., C.T., G.Y., and X.L. analyzed the data; G.C. and L.F. provided the study materials; D.C., Y.T., and X.L. wrote the manuscript.
The author responsible for distribution of materials integral to the findings presented in this article in accordance with the policy described in the Instructions for Authors (https://academic.oup.com/plphys/pages/general-instructions) is: Xiang-Dong Li (xdongli@sdau.edu.cn).

Abstract

Chloroplasts play an indispensable role in the arms race between plant viruses and hosts. Chloroplast proteins are often recruited by plant viruses to support viral replication and movement. However, the mechanism by which chloroplast proteins regulate potyvirus infection remains largely unknown. In this study, we observed that *Nicotiana benthamiana* ribosomal protein large subunit 1 (NbRPL1), a chloroplast ribosomal protein, localized to the chloroplasts via its N-terminal 61 amino acids (transit peptide), and interacted with tobacco vein banding mosaic virus (TVBMV) nuclear inclusion protein b (NIb), an RNA-dependent RNA polymerase. Upon TVBMV infection, NbRPL1 was recruited into the 6K2-induced viral replication complexes in chloroplasts. Silencing of *NbRPL1* expression reduced TVBMV replication. NbRPL1 competed with NbBeclin1 to bind NIb, and reduced the NbBeclin1-mediated degradation of NIb. Therefore, our results suggest that NbRPL1 interacts with NIb in the chloroplasts, reduces NbBeclin1-mediated NIb degradation, and enhances TVBMV infection.

Introduction

Chloroplasts are organelles that conduct photosynthesis by trapping energy from sunlight, and are the site of synthesis for key biochemical components. Chloroplasts are also targets of plant viruses (Li et al., 2016; Zhao et al., 2016; Bhattacharyya and Chakraborty, 2018). Viral infections cause a substantial reduction in photosynthesis (Montasser et al., 2012; Bhattacharyya et al., 2015; Li et al., 2016; Zhao et al., 2016), and expression of chloroplast-related genes is affected during viral infection (Li et al., 2016). Chlorosis in *Nicotiana benthamiana* leaves caused by the rice stripe virus is due to the downregulation of chloroplast-related gene expression (Shi et al., 2016). Our previous study showed that tobacco vein banding mosaic virus (TVBMV) infection causes differential expression of many chloroplast-related genes in *N. benthamiana* (Geng et al., 2017).

Received March 12, 2021. Accepted May 06, 2021. Advance access publication May 31, 2021

Chloroplast proteins are involved in several viral infection processes, including replication and movement. The *N. benthamiana* chloroplast protein glyceraldehyde 3-phosphate dehydrogenase subunit A (NbGAPDH-A) interacts with the movement protein (MP) of red clover necrotic mosaic virus, and silencing of *NbGAPDH-A* expression inhibits MP localization to cortical viral replication complexes (VRCs) and chloroplasts (Kaido et al., 2014). Chloroplast phosphoglycerate kinase (chl-PGK) is used by the bamboo mosaic virus (BaMV) RNA to target chloroplasts; knocking down the expression levels of chl-PGK reduced BaMV coat protein (CP) accumulation (Cheng et al., 2013). The *N. benthamiana* rubisco small subunit (NbRbCS) interacts with the MP of tomato mosaic virus; silencing of *NbRbCS* expression was reported to delay the appearance of systemic symptoms (Zhao et al., 2013). The expression levels of the chloroplast ATP-synthase γ-subunit (AtpC) and rubisco activase are reduced in tobacco mosaic virus-infected *N. benthamiana* plants, and silencing either gene enhanced viral accumulation (Bhat et al., 2013).

Potyviruses (genus *Potyvirus*, family *Potyviridae*) form the largest plant RNA virus group, and cause substantial economic losses to crop production worldwide (Ivanov et al., 2014). The potyvirus genome is a positive-sense single-stranded RNA that encodes 11 proteins (Chung et al., 2008; Revers and García, 2015). Among these viral proteins, nuclear inclusion protein b (NIb) is an RNA-dependent RNA polymerase that contains a conserved GDD motif (Koonin, 1991). A previous study has shown that the light-induced protein localizes in chloroplasts and interacts with wheat yellow mosaic virus NIb to facilitate viral infection (Zhang et al., 2019). Cytoplasmic ribosomal protein P0 is present in the ribonucleoprotein complexes that can be immunoprecipitated using potato virus A (PVA) NIb and promotes PVA infection (Hafrén et al., 2013). However, no chloroplast ribosomal protein has been reported to interact with NIb.

In this study, we determined that the *N. benthamiana* chloroplast ribosomal protein larger subunit 1 (NbRPL1) can interact with TVBMV NIb. Further, we studied the function of NbRPL1 in the infection of TVBMV.

Results

TVBMV NIb interacts with chloroplast protein NbRPL1

Interaction between chloroplast proteins and TVBMV NIb was determined after extracting total protein from *N. benthamiana* leaves transiently expressing MYC:NIb. Total protein was immunoprecipitated with anti-MYC agarose beads, and separated by sodium dodecyl sulphate-polyacrylamide gel electrophoresis (SDS–PAGE). The co-precipitated proteins in the gel were identified by liquid chromatography tandem mass spectrometry followed by database searches. Two chloroplast proteins, the 50S ribosomal protein large subunit 1 (NbRPL1) and the elongation factor Tu (NbEF-Tu) of *N. benthamiana*, were selected for further analyses due to their high confidence and peptide coverage (Supplemental Figure S1).

Pull-down and bimolecular fluorescence complementation (BiFC) assays were then conducted to investigate whether NbRPL1 or NbEF-Tu interacted directly with TVBMV NIb. HIS:eGFP:NbRPL1 and HIS:MBP:MYC:NIb, HIS:eGFP:NbEF-Tu and HIS:MBP:MYC:NIb, and HIS:eGFP and HIS:MBP:MYC:NIb were incubated with GFP-Trap_A beads, respectively, followed by western blotting. Results showed that TVBMV NIb interacted directly with NbRPL1, but not with NbEF-Tu (Figure 1A). To further verify the interaction between NIb and NbRPL1, we transiently co-expressed NIb:YN and NbRPL1:YC, NIb:YN and YC, or YN and NbRPL1:YC in *N. benthamiana* leaves. Confocal microscopy revealed YFP fluorescence in the chloroplasts in *N. benthamiana* leaf cells co-expressing NIb:YN and NbRPL1:YC (Figure 1B). Both pull-down and BiFC assays showed that TVBMV NIb interacted with NbRPL1 directly. Transient expression of NbRPL1:DsRed or NbRPL1:eGFP in *N. benthamiana* leaves revealed that NbRPL1 was localized in chloroplasts (Figure 1C).

Chloroplast transit peptide domain is required for NbRPL1 chloroplast targeting

The chloroplast transit peptide (cTP) plays an important role in targeting proteins to chloroplasts (Bionda et al., 2010). We predicted the potential function of NbRPL1 cTP using the ChloroP 1.1 server (http://www.cbs.dtu.dk/services/ChloroP/; Emanuelsson et al., 1999). The result showed that the N-terminal 61 amino acids (aa) could form the cTP of NbRPL1, with the cleavage-site motif of Val-Val-Ala↓Ala (Figure 2A). To verify the cleavage activity of NbRPL1 in vivo, we expressed NbRPL1:DsRed in healthy and TVBMV-infected *N. benthamiana* plants. Total protein extracts were incubated with anti-mCherry beads, followed by SDS–PAGE. Two bands of about 64.1 kDa and 57.7 kDa, corresponding to the size of NbRPL1:DsRed with or without cTP (NbRPL1:DsRed and NbRPL1$^{\Delta cTP}$:DsRed), respectively, were observed in both treatments (Figure 2B).

Mapping of the key region in cTP that regulates NbRPL1 chloroplast targeting was performed through transient expression of NbRPL1$^{\Delta cTP(N61aa)}$:DsRed, NbRPL1$^{\Delta N41aa}$:DsRed, NbRPL1$^{\Delta N20aa}$:DsRed, NbRPL1$^{\Delta N42-61aa}$:DsRed, NbRPL1$^{\Delta N21-61aa}$:DsRed, or NbRPL1$^{\Delta N21-41aa}$:DsRed in *N. benthamiana* leaves. Confocal microscopy revealed that none of the truncated mutants were located in chloroplasts, indicating that the integrity of cTP is crucial for NbRPL1 chloroplast targeting (Figure 2, C and D).

We also investigated the role of the C-terminal aa in NbRPL1 chloroplast targeting. Transient expression of the truncated mutant NbRPL1$^{\Delta 1-280aa}$:DsRed (expressing C-terminal 60 aa) or NbRPL1$^{\Delta 281-340aa}$:DsRed (expressing N-terminal 280 aa) in *N. benthamiana* leaves showed that NbRPL1$^{\Delta 281-340aa}$:DsRed was localized in chloroplasts, whereas NbRPL1$^{\Delta 1-280aa}$:DsRed was localized in cytoplasm, indicating that the C-terminal aa was dispensable for NbRPL1 chloroplast targeting (Figure 2, C and E).

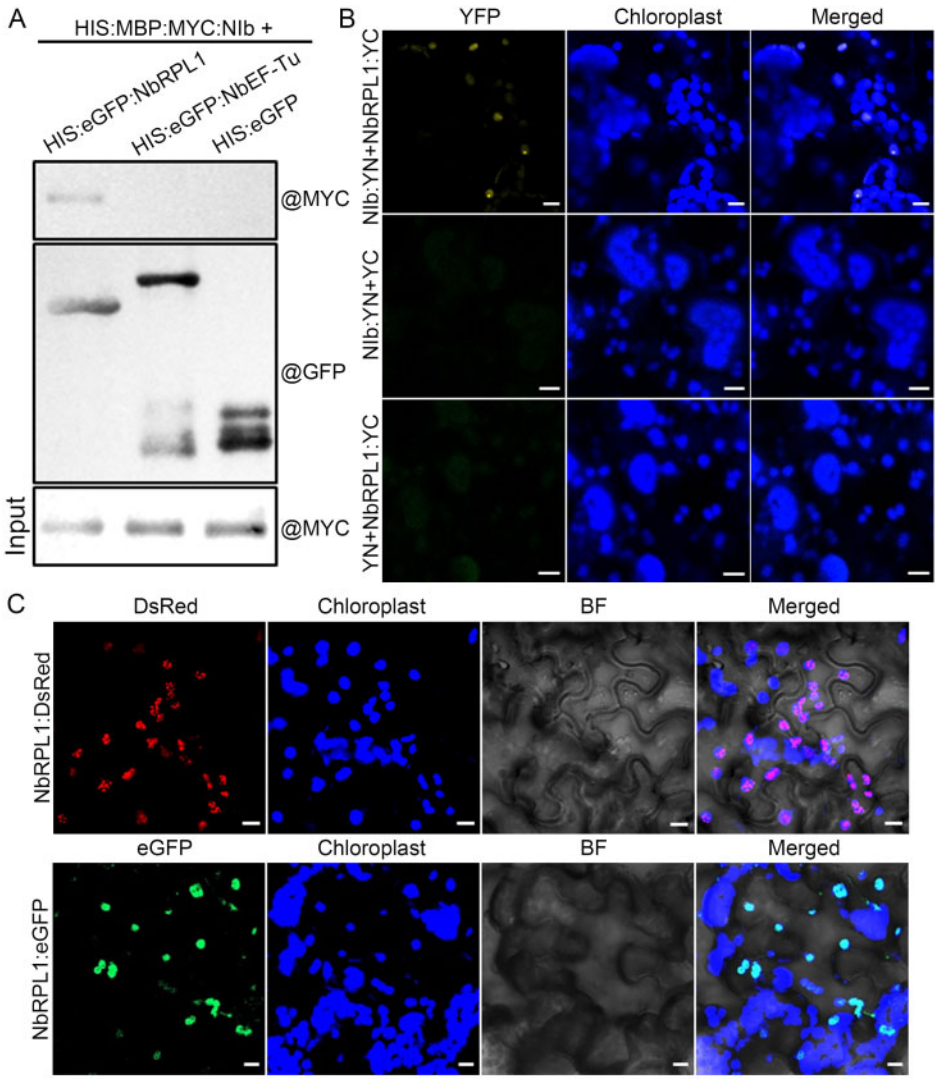

Figure 1 NbRPL1 physically interacts with TVBMV NIb in vitro and in vivo. A, Determination of interactions between HIS:eGFP:NbRPL1, HIS:eGFP:NbEF-Tu, and HIS:MBP:MYC:NIb using in vitro pull-down assay. The combination of HIS:eGFP and HIS:MBP:MYC:NIb was used as the negative control. Pull-down assays were performed using GFP-Trap_A beads followed by Western blotting analyses using an MYC-specific or a GFP-specific antibody. B, BiFC analysis of the interaction between NIb:YN and NbRPL1:YC in *N. benthamiana* leaf cells. Co-expression of NIb:YN and YC or YN and NbRPL1:YC were used as negative controls. C, Confocal micrographs of *N. benthamiana* leaves agroinfiltrated with plasmids expressing NbRPL1:eGFP or NbRPL1:DsRed. Images of *N. benthamiana* leaf cells were taken at 36 hpai. Scale bars = 10 μm.

We then co-expressed NIb:YN and NbRPL1$^{\Delta cTP}$:YC, or YN and NbRPL1$^{\Delta cTP}$:YC in *N. benthamiana* leaves to investigate whether cTP is required for the interaction between NbRPL1 and NIb. The result showed that NIb:YN interacted with NbRPL1$^{\Delta cTP}$:YC (Figure 2F), indicating that cTP is dispensable for the interaction between NIb and NbRPL1.

The NbRPL1/NIb complex co-localizes with the 6K2-associated VRCs in TVBMV-infected cells

It was worth investigating whether NbRPL1 was also present in the TVBMV VRCs. We transiently co-expressed NIb:YN, NbRPL1:YC, and 6K2:DsRed in *N. benthamiana* leaves, and found that NbRPL1 and NIb co-localized in the 6K2-induced vesicles (Figure 3A). We also transiently co-expressed NbRPL1:YC and NIb:YN with the nuclear marker H2B:mCherry or the plasmodesmata marker, *Arabidopsis thaliana* plasmodesmata-localized protein 1 (AtPDLP1), AtPDLP1:DsRed in *N. benthamiana* leaves. The result showed that the NIb/NbRPL1 complex was not localized in the nucleus or plasmodesmata (Figure 3B). Further, in the presence of TVBMV infection, NIb and NbRPL1 co-localized with the 6K2-induced VRCs in chloroplasts (Figure 3C).

Silencing of *NbRPL1* expression reduces TVBMV systemic movement and replication

The role of *NbRPL1* in TVBMV infection in plants was investigated through silencing *NbRPL1* expression in *N. benthamiana* using a tobacco rattle virus (TRV)-based virus-induced gene silencing (VIGS) vector, and subsequently inoculating these *NbRPL1*-silenced plants with TVBMV-GFP. The

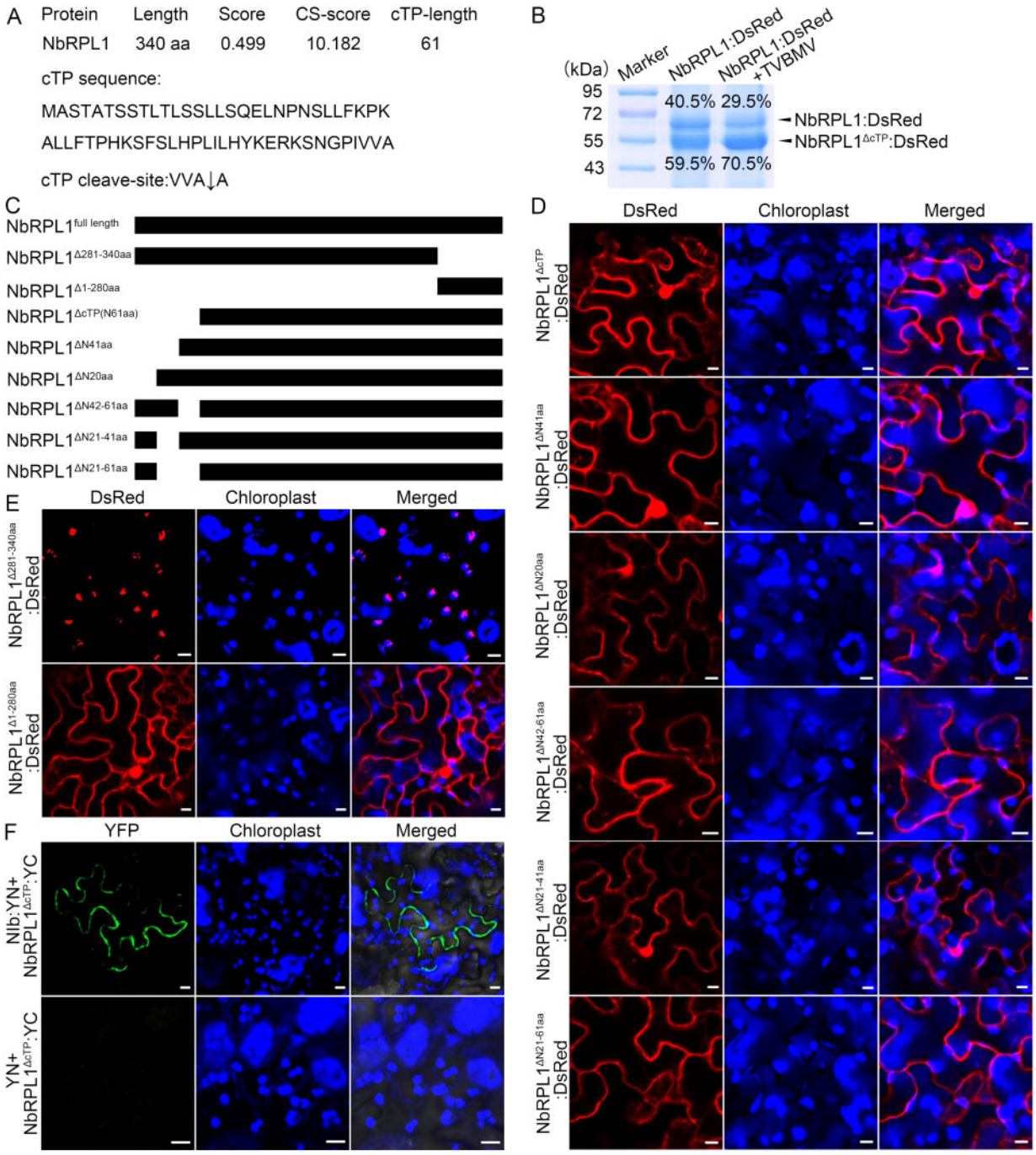

Figure 2 Identification of the cTP domain, and its effects on the subcellular distribution of NbRPL1 and the interaction between NIb and NbRPL1. A, Prediction of cTP in NbRPL1. B, SDS–PAGE analysis of NbRPL1:DsRed expressed in the noninfected and TVBMV-infected *N. benthamiana* leaves. Sizes of the bands of the molecular weight marker are shown on the left. C, Schematic representations of NbRPL1 and its deletion mutants. D and E, Confocal micrographs of *N. benthamiana* leaf cells expressing NbRPL1$^{\Delta cTP(N61aa)}$:DsRed, NbRPL1$^{\Delta N41aa}$:DsRed, NbRPL1$^{\Delta N20aa}$:DsRed, NbRPL1$^{\Delta N42-61aa}$:DsRed, NbRPL1$^{\Delta N21-61aa}$:DsRed, and NbRPL1$^{\Delta N21-42aa}$:DsRed (D), and NbRPL1$^{1-280aa}$:DsRed and NbRPL1$^{281-340aa}$:DsRed (E). F, BiFC analysis of the interaction between NIb:YN and NbRPL1$^{\Delta cTP}$:YC. Co-expression of YN and NbRPL1$^{\Delta cTP}$:YC was used as a negative control. Images of *N. benthamiana* leaf cells were captured under a confocal microscope at 36 hpai. Scale bars = 10 μm.

NbRPL1-silenced *N. benthamiana* plants showed etiolation of systemic leaves by 8 d post virus inoculation through agroinfiltration (Figure 4A). Reverse transcription quantitative polymerase chain reaction (RT-qPCR) analysis showed that at 8 d post agroinfiltration (dpai), the accumulation of *NbRPL1* mRNA in the *NbRPL1*-silenced *N. benthamiana* plants was ∼10% of that in the control plants (Figure 4B). At 6 d post-TVBMV-GFP inoculation, UV illumination induced green fluorescence in the systemic leaves of the TRV-GUS-treated (control) plants, but not in the *NbRPL1*-

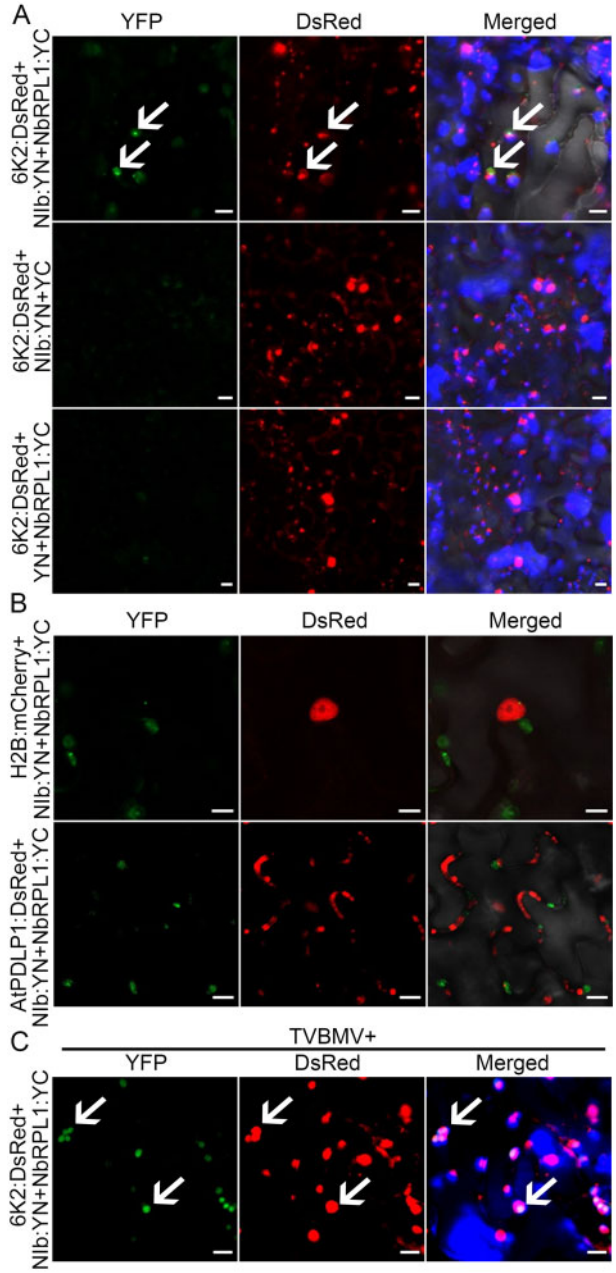

Figure 3 The NbRPL1/NIb complex co-localizes with TVBMV 6K2 on chloroplasts upon TVBMV infection. A, Co-localization of NIb:YN, NbRPL1:YC, and 6K2:DsRed in *N. benthamiana* leaf cells. Co-expressions of NIb:YN, YC, and 6K2:DsRed or YN, NbRPL1:YC, and 6K2:DsRed were used as negative controls. White arrowheads indicate the co-localization of the NIb:YN/NbRPL1:YC complex with 6K2:DsRed. B, Subcellular distributions of NIb:YN, NbRPL1:YC, and H2B:mCherry or NIb:YN, NbRPL1:YC, and AtPDLP1:DsRed in *N. benthamiana* leaf cells. H2B:mCherry is a nuclear marker and AtPDLP1:DsRed is a plasmodesmata marker. C, Co-localization of NIb:YN, NbRPL1:YC, and 6K2:DsRed in the TVBMV-infected *N. benthamiana* leaf cells. White arrowheads indicate the co-localization of the NIb:YN/NbRPL1:YC complex with 6K2:DsRed. Images were taken under a confocal microscope at 36 hpai. Scale bars = 10 μm.

silenced plants (Figure 4C). Western blotting result showed that TVBMV CP had accumulated in the systemic leaves of the control plants, but not in the systemic leaves of the *NbRPL1*-silenced plants (Figure 4D). Reverse transcription semi-quantitative PCR (RT-sqPCR) result showed that viral RNA was present in the systemic leaves of the control plants, but not in the systemic leaves of the *NbRPL1*-silenced plants (Figure 4E). These results suggest that silencing *NbRPL1* abolished TVBMV long-distance movement.

The effect of *NbRPL1* silencing on TVBMV accumulation and replication in the inoculated leaves was determined through inoculation of TVBMV-GFP to *NbRPL1*-silenced and nonsilenced *N. benthamiana* leaves via agroinfiltration. At 72-h post agroinfiltration (hpai), the TVBMV-GFP-inoculated control leaves showed stronger green fluorescence than the TVBMV-GFP-inoculated *NbRPL1*-silenced leaves (Figure 4F). Western blotting analysis indicated that TVBMV CP accumulation was reduced in the *NbRPL1*-silenced *N. benthamiana* leaves (Figure 4G). RT-sqPCR showed that the accumulation level of TVBMV-GFP viral RNA was reduced in the inoculated leaves of the *NbRPL1*-silenced plants (Figure 4H). We also inoculated the *NbRPL1*-silenced and nonsilenced control *N. benthamiana* leaves with TVBMV$^{\Delta P3NPIPO}$-GFP, a mutant defective for cell-to-cell movement, to exclude the effect of intracellular viral movement on RNA accumulation. The RT-qPCR assays showed that the level of TVBMV$^{\Delta P3NPIPO}$-GFP viral RNA in the leaves of the *NbRPL1*-silenced plants was significantly reduced compared to the nonsilenced control plant by 36 hpai (Figure 4I).

The effect of *NbRPL1* on the subcellular localization of 6K2-induced vesicles was investigated by transient expression of 6K2:DsRed in *NbRPL1*-silenced leaves. Confocal microscopy showed that 6K2:DsRed was localized in the chloroplasts of the *NbRPL1*-silenced and control plants (Figure 4J). To investigate whether silencing of *NbRPL1* expression affects the recruitment of NIb to VRC in TVBMV infection, we co-expressed NIb:mCherry and TVBMV-6K2:GFP in the leaves of the *NbRPL1*-silenced and control plants. We found that NIb:mCherry co-localized with 6K2 in the chloroplasts in control leaves. However, the co-localization of NIb and VRC was reduced in the *NbRPL1*-silenced plant leaves (Figure 4K). The result showed that silencing of *NbRPL1* expression did not affect the localization of 6K2:DsRed in chloroplasts, but reduced the co-localization of NIb and VRCs in chloroplasts during TVBMV infection.

Overexpression of *NbRPL1* increases the accumulation of TVBMV NIb and RNA

The effect of *NbRPL1* overexpression on TVBMV infection was determined through agroinfiltration of TVBMV-GFP into NbRPL1-overexpressing *N. benthamiana* leaves. At 96 hpai, representative TVBMV-GFP infection foci in the infiltrated leaves were photographed under a stereo fluorescence microscope (Figure 5A). The mean number of TVBMV-GFP-infected cells in each infection site in the NbRPL1-overexpressed leaves was 47 ± 20, whereas that in

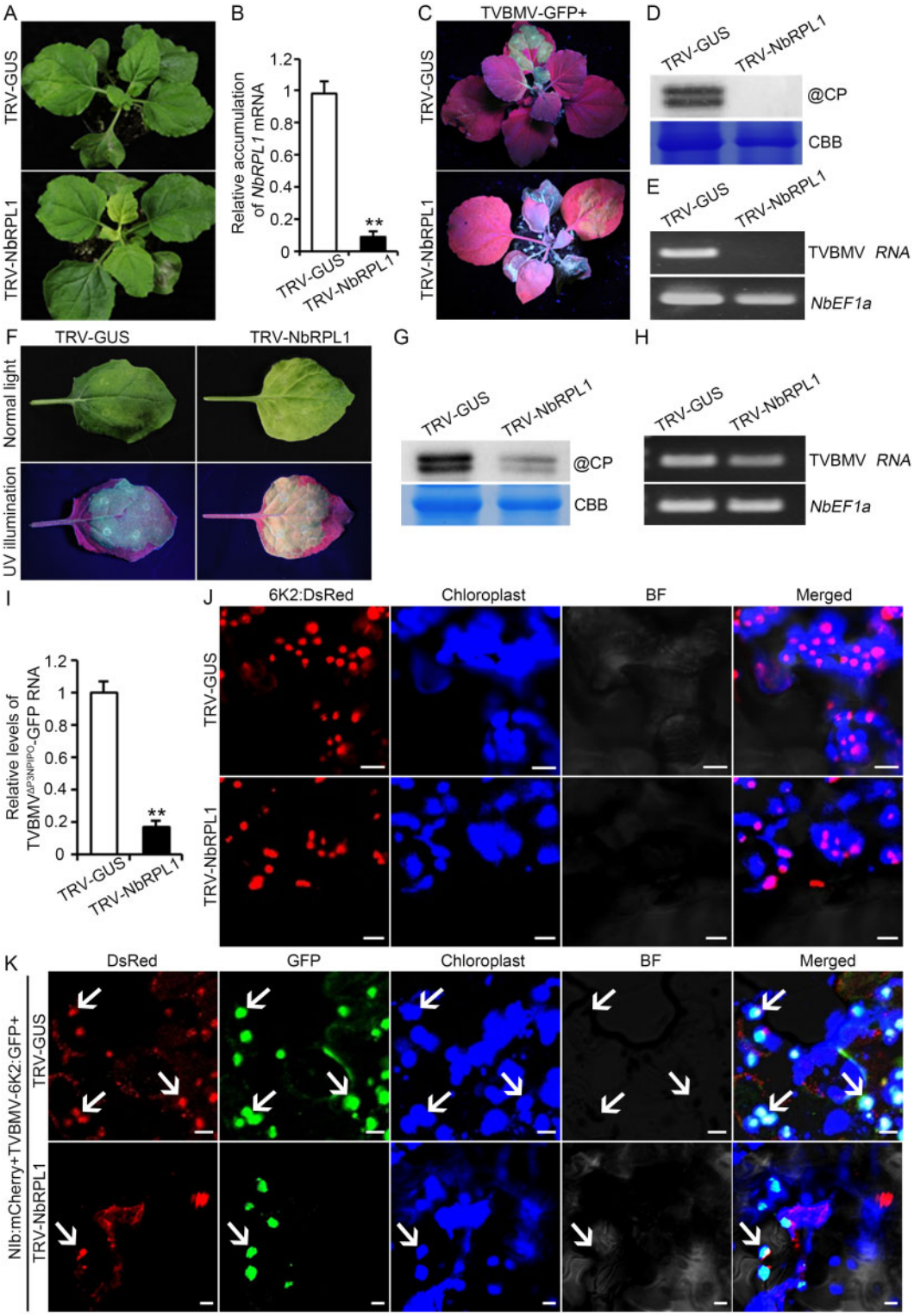

Figure 4 Silencing of *NbRPL1* expression affects TVBMV infection and the subcellular distribution of NIb in *N. benthamiana* plants. A, Phenotypes of the *NbRPL1*-silenced (TRV-NbRPL1) and nonsilenced (TRV-GUS) *N. benthamiana* plants at 8 dpai. B, Relative expression of *NbRPL1* in the systemic leaves of the *NbRPL1*-silenced and nonsilenced *N. benthamiana* plants was determined through RT-qPCR. Error bars indicate the standard deviations of three biological replicates per treatment. Statistical significance was determined using a two-tailed Student's *t* test (**$P < 0.01$). C, Phenotypes of the *NbRPL1*-silenced and nonsilenced *N. benthamiana* plants at 6 d post TVBMV-GFP inoculation (dpi). Plants were photographed under UV illumination. D, Western blotting analysis of TVBMV CP accumulation in the systemic leaves of the TVBMV-GFP-inoculated *NbRPL1*-silenced or nonsilenced *N. benthamiana* plants at 6 d post TVBMV-GFP inoculation. The Coomassie Brilliant Blue R-250 (CBB)-stained gel shows sample loadings. E, RT-PCR detection of TVBMV RNA accumulation in the systemic leaves of the TVBMV-GFP-inoculated *NbRPL1*-silenced or nonsilenced *N. benthamiana* plants at 6 dpi using TVBMV CP gene specific primers. F, GFP fluorescence in the *NbRPL1*-silenced *N. benthamiana* leaves. Images of TVBMV-GFP-inoculated nonsilenced or *NbRPL1*-silenced leaves were taken under normal light or UV illumination at 72 hpai. G, Western blotting analysis of TVBMV CP accumulation in the TVBMV-GFP-inoculated *NbRPL1*-silenced or nonsilenced *N. benthamiana* leaves at

the control leaves was 31 ± 14 (Figure 5, A and B), indicating that the overexpression of NbRPL1 in *N. benthamiana* leaves enhanced virus cell-to-cell movement. We also agroinfiltrated the leaves of the NbRPL1-overexpression and control plants with TVBMV$^{\Delta GDD}$-RLUC//FLUC. Results of the dual-luciferase activity assay showed that, by 60 hpai, the activities of Renilla luciferase (Rluc) and Firefly luciferase (Fluc) from TVBMV$^{\Delta GDD}$-RLUC//FLUC (Supplemental Figure S2) in the NbRPL1-overexpression *N. benthamiana* leaves was similar to that in the leaves of the control plants (Figure 5C), indicating that overexpression of NbRPL1 did not affect the translation efficiency.

TVBMV-GFP was transfected into the protoplasts isolated from the NbRPL1-overexpression or control *N. benthamiana* leaves to investigate the effect of NbRPL1 on TVBMV replication. Viral RNA accumulation was detected through RT-qPCR at 12-h post transfection. The results showed that TVBMV RNA accumulation in the NbRPL1-overexpression protoplasts was significantly higher than that in the control protoplasts (Figure 5D). We then agroinfiltrated TVBMV$^{\Delta P3NPIPO}$-GFP into the NbRPL1-overexpression and control *N. benthamiana* leaves. RT-qPCR results showed that, by 36 hpai, TVBMV RNA accumulation in the NbRPL1-overexpressing leaves was significantly higher than that in the control (Figure 5E), indicating that NbRPL1 could enhance TVBMV replication.

The effect of NbRPL1 on TVBMV NIb accumulation was determined through co-expressing NbRPL1:DsRed and MYC:NIb in the TVBMV-infected *N. benthamiana* leaves. Western blotting result showed that NIb accumulation in the NbRPL1-overexpressing *N. benthamiana* leaves was higher than that in the control *N. benthamiana* leaves (Figure 5F).

These results showed that overexpression of NbRPL1 promoted the accumulation of NIb and viral RNA, which promoted the cell-to-cell movement of TVBMV.

NbRPL1 interferes with the binding and degradation of NIb by NbBeclin1

Eight autophagy-related genes (ATGs): namely, *NbATG2*, *NbATG3*, *NbATG4*, *NbATG8a*, *NbATG8c*, *NbATG8i*, *NbBeclin1*, and *NbVPS15*, were upregulated in the TVBMV-infected plants at 7 and 16 dpi, as indicated by RT-qPCR analysis (Supplemental Figure S3, A and B), suggesting that TVBMV infection could activate the autophagy pathway. To verify whether NbBeclin1 could recognize TVBMV NIb, we performed co-immunoprecipitation (Co-IP), yeast two-hybrid (Y2H), and BiFC assays. The results showed that NbBeclin1 interacted with TVBMV NIb in vitro and in vivo (Figure 6, A–C). NbBeclin1:eGFP and MYC:NIb were co-expressed in *N. benthamiana* leaves to ascertain whether NbBeclin1 could mediate the degradation of TVBMV NIb. Western blotting result showed that MYC:NIb accumulation in the *N. benthamiana* leaves overexpressing NbBeclin1:eGFP was reduced compared to that in the control plants (Figure 6D), indicating that overexpression of NbBeclin1 could enhance the degradation of TVBMV NIb. The RT-qPCR results showed that, by 2 dpai, the accumulation level of TVBMV RNA in the NbBeclin1-overexpressing leaves was significantly lower than that in the control (Figure 6E), indicating that NbBeclin1 could reduce TVBMV replication. These results indicate that TVBMV infection can activate the autophagy pathway, and NbBeclin1 can interact with NIb and mediate its degradation.

The role of NbRPL1 in NbBeclin1-mediated *in vivo* degradation of NIb was determined through co-expressing NbBeclin1:eGFP, MYC:NIb, and HA:NbRPL1 in *N. benthamiana* leaves. Western blotting result showed that MYC:NIb accumulation in the HA:NbRPL1-overexpressing leaves was higher than that in the control plant leaves (Figure 6F), indicating that NbRPL1 overexpression reduced the NbBeclin1-mediated degradation of NIb. The RT-qPCR results showed that, by 2 dpai, the accumulation level of TVBMV RNA in the HA:NbRPL1- and NbBeclin1-overexpressing *N. benthamiana* leaves was significantly higher than that in the NbBeclin1-overexpressing *N. benthamiana* leaves (Figure 6G). These results indicated that NbRPL1 could promote TVBMV replication through reducing the degradation of NIb by NbBeclin1.

Considering that both NbRPL1 and NbBeclin1 can bind TVBMV NIb, it is reasonable to hypothesize that NbRPL1 interferes the NbBeclin1-mediated NIb degradation through competing with NbBeclin1 for NIb. We conducted a pull-down assay to determine the effect of NbRPL1 on NbBeclin1 and NIb interaction. Mixtures with HIS:MBP:MYC:NIb, HIS:eGFP:NbBeclin1, and different concentrations of HIS:HA:NbRPL1 were incubated with GFP-Trap_A beads followed by western blotting analyses using MYC-, HA-, and GFP-specific antibodies. The results showed that increase of HIS:HA:NbRPL1 concentration reduced the amount of HIS:MBP:MYC:NIb bound by HIS:eGFP:NbBeclin1 (Figure 6H). These results indicate that NbRPL1 can compete with NbBeclin1 for TVBMV NIb in vitro.

Discussion

In this study, we determined that chloroplast ribosomal protein NbRPL1 interacts with TVBMV NIb in the 6K2-associated VRCs in chloroplasts. The cTP transit peptide domain

72 hpai. The CBB-stained gel shows sample loadings. H, RT-PCR detection of TVBMV RNA accumulation in the TVBMV-GFP-inoculated *NbRPL1*-silenced or nonsilenced *N. benthamiana* leaves at 72 hpai using the TVBMV CP gene specific primers. I, RT-qPCR analysis of TVBMV$^{\Delta P3NPIPO}$-GFP RNA accumulation in the TVBMV-GFP-inoculated *NbRPL1*-silenced or nonsilenced *N. benthamiana* leaves at 36 hpai using the TVBMV CP gene specific primers. Error bars indicate the standard deviation of three biological replicates per treatment. Statistical significance was determined using a two-tailed Student's *t* test (**$P < 0.01$). J, Localization of 6K2:DsRed in the *NbRPL1*-silenced or nonsilenced *N. benthamiana* leaves. K, Co-localization of NIb:mCherry and TVBMV-6K2:GFP in the *NbRPL1*-silenced or nonsilenced *N. benthamiana* leaves. White arrowheads indicate the co-localization of 6K2:GFP and NIb:mCherry. Scale bars = 10 μm.

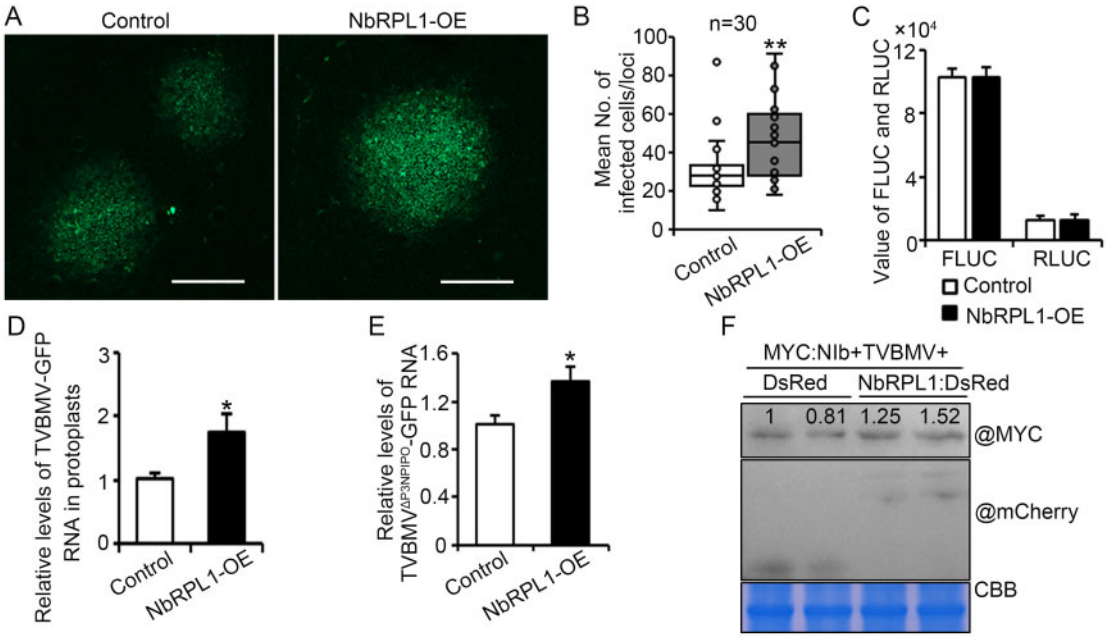

Figure 5 The overexpression of NbRPL1 in *N. benthamiana* leaves increases TVBMV cell-to-cell movement and RNA accumulation, and increases the accumulation of TVBMV NIb. A, Micrographs of TVBMV-GFP cell-to-cell movement in the control and NbRPL1-overexpressing *N. benthamiana* leaves. Images were taken at 96 hpai. Green fluorescence represents the GFP-tagged TVBMV. Scale bars = 500 μm. B, The mean number of TVBMV-GFP-infected cells in each examined field. The number of TVBMV-GFP-infected cells in each locus was counted under the stereo fluorescence microscope. For each treatment, 30 infection loci were counted. In the NbRPL1-overexpressing experiment, the boxplots represent the data dispersion around the median with the position of the lower limit value (18), the lower quartile (28.5), the median (45.5), the upper quartile (58.75), and the upper limit value (91). In the control, the boxplots represent the data dispersion around the median with the position of the lower limit value (10), the lower quartile (23), the median (28), the upper quartile (33), and the upper limit value (46). Statistical significance was calculated using a two-tailed Student's *t* test (**$P < 0.01$). C, Effect of NbRPL1 overexpression on viral protein translation efficiency in *N. benthamiana* leaves. Relative activities of RLUC and FLUC in the pCB301TVBMV$^{\Delta GDD}$-RLUC//FLUC-inoculated leaves were determined at 60 hpai. Error bars indicate the standard deviation of three biological replicates per treatment. D, RT-qPCR detection of TVBMV genomic RNA in the NbRPL1-overexpressing and control *N. benthamiana* protoplasts using TVBMV *CP* gene-specific primers. Expression of *NbEF1α* was used as an internal control. Error bars indicate the standard deviation of three biological replicates per treatment. Statistical significance was determined using a two-tailed Student's *t* test (*$P < 0.05$). E, RT-qPCR detection of TVBMV$^{\Delta P3NPIPO}$-GFP RNA in the NbRPL1-overexpressing or control *N. benthamiana* leaves using TVBMV CP gene specific primers. Expression of *NbEF1α* was used as an internal control. Error bars indicate the standard deviation of three biological replicates per treatment. Statistical significance was calculated using a two-tailed Student's *t* test (*$P < 0.05$). F, Western blotting detection of MYC:NIb co-expressed with NbRPL1:DsRed or DsRed in the TVBMV-infected *N. benthamiana* leaves at 2 dpai using MYC-specific and mCherry-specific antibodies, respectively. Band intensities were measured using the ImageJ software. The CBB-stained gel shows sample loadings.

of NbRPL1 is essential for the NbRPL1 chloroplast targeting. We also observed that NbRPL1 could reduce the degradation of NIb through interfering with the NbBeclin1-mediated autophagy pathway to promote TVBMV infection. This research advances our understanding of the roles of chloroplast ribosomal proteins in potyviral pathogenesis, and provides a target for engineering resistance to potyviruses.

Chloroplasts are important host organelles where many interactions between host factors and pathogens occur. Several chloroplast localized viral proteins have been shown to play critical roles in viral infection (Zhao et al., 2016; Bhattacharyya and Chakraborty, 2018). Potyviruses form VRCs and replicate their genomes in chloroplasts. Potyvirus 6K2-induced VRCs are transported from endoplasmic reticulum (ER) to chloroplasts via vesicular transport and actomyosin motility systems (Wei et al., 2010). The ER-localized soluble N-ethylmaleimide-sensitive-factor attachment protein receptors protein Syp71 has been shown to co-localize with *Turnip mosaic virus* (TuMV) 6K2 in chloroplasts to mediate the fusion of viral VRCs with chloroplasts. Silencing of *Syp71* expression arrested the formation of chloroplast-bound 6K2 complexes, and inhibited viral infection (Wei et al., 2013). Our previous study also showed that TVBMV 6K2 recruited chloroplast NbPsbO1, the Photosystem II oxygen evolution complex protein of *N. benthamiana*, for virus replication, and knockdown of *NbPsbO1* expression inhibited TVBMV and *Potato virus Y* replication in plants (Geng et al., 2017). In this study, we found that NbRPL1, a 50S ribosomal protein L1, accumulates in chloroplasts and interacts with TVBMV NIb (Figure 1). During TVBMV infection in the plant, viral NIb hijacks NbRPL1 into the VRCs to ensure viral replication (Figure 3). Overexpression of NbRPL1 promoted viral replication and cell-to-cell movement, but not translation, while

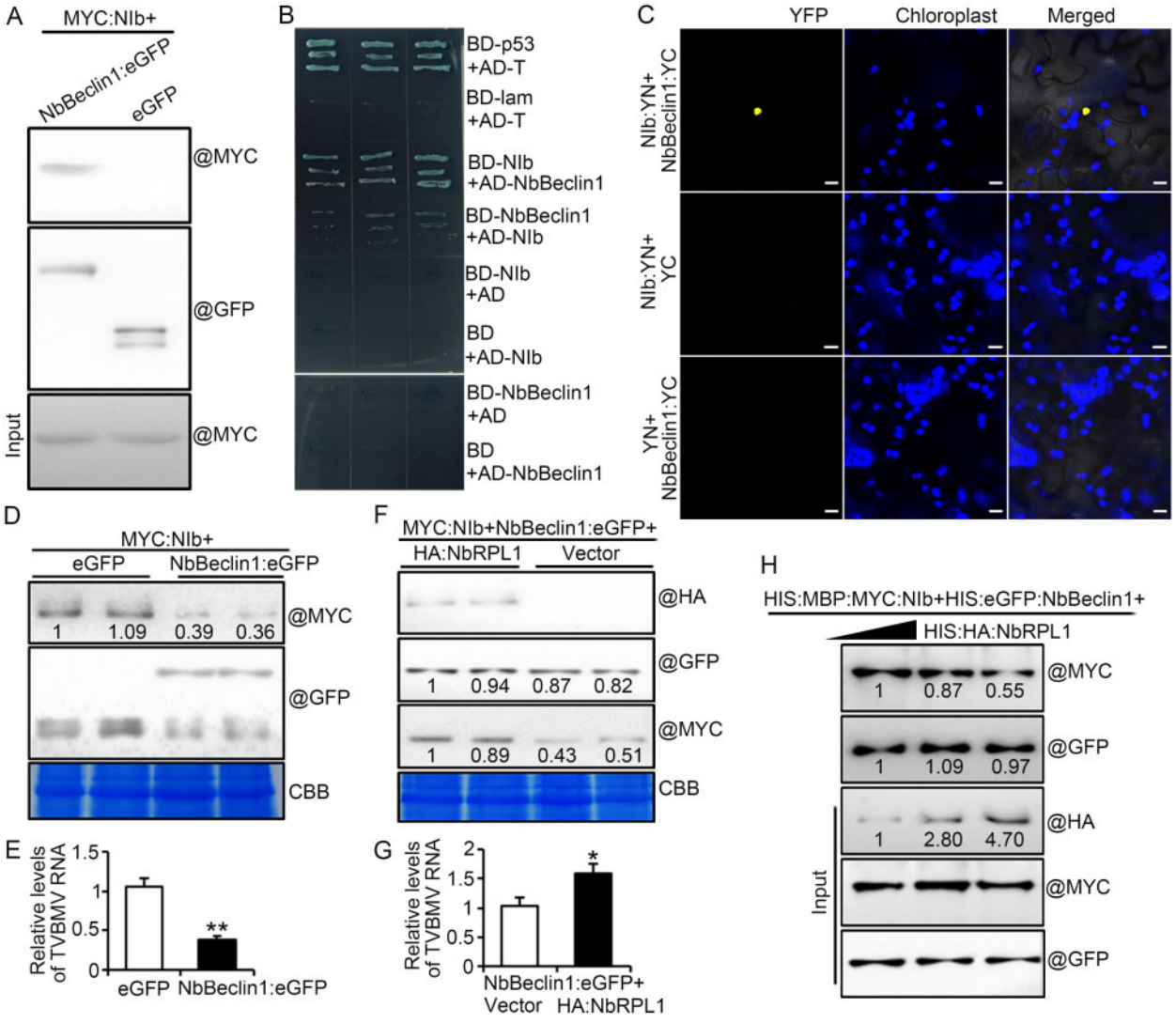

Figure 6 NbRPL1 competes with NbBeclin1 for NIb. A, Co-IP analysis of NbBeclin1:eGFP and MYC:NIb in vivo interaction. Combination of eGFP and MYC:NIb was used as the negative control. The Co-IP analysis was performed with GFP-Trap_A beads followed by western blotting detection using an MYC-specific antibody. B, Determination of NIb and NbBeclin1 interaction through Y2H assay. Yeast cells were co-transformed with BD-NIb and AD-NbBeclin1 or AD-NIb and BD-NbBeclin1. The transformed cells were grown on the SD/-Trp/-Leu/-His/-Ade selection medium supplemented with X-α-Gal for 4 d. Y2H cells co-transformed with AD-T-ant and BD-p53 were used as the positive control, whereas Y2H cells co-transformed with AD-T-ant and BD-lam, BD-NIb and AD, AD-NIb and BD, BD and AD-NbBeclin1, or AD and BD-NbBeclin1 were used as negative controls. BD, pGBKT7; AD, pGADT7. C, BiFC analysis of NIb:YN and NbBeclin1:YC interaction in *N. benthamiana* leaves. NIb:YN and YC or YN and NbBeclin1:YC co-expressing *N. benthamiana* leaves were used as negative controls. Confocal images of leaf cells were taken at 36 hpai. Scale bars = 10 μm. D, Western blotting assay of total protein extracts from *N. benthamiana* leaves co-expressing NbBeclin1:eGFP and MYC:NIb using a GFP specific or a MYC specific antibody at 2 dpai. A *N. benthamiana* leaf sample co-expressing NbBeclin1:eGFP and MYC:NIb was used as the negative control. The CBB-stained gel shows sample loadings. E, RT-qPCR detection of TVBMV RNA in the *N. benthamiana* leaves co-expressing TVBMV and NbBeclin1:eGFP at 2 dpai. Co-expression of TVBMV and eGFP in *N. benthamiana* leaves was used as the negative control. Expression of *NbEF1α* was used as an internal control. Error bars indicate the standard deviation of three biological replicates per treatment. Statistical significance was determined using a two-tailed Student's *t* test (**$P < 0.01$). F, Western blotting analysis of total protein extracts from *N. benthamiana* leaves co-expressing HA:NbRPL1, NbBeclin1:eGFP, and MYC:NIb using a HA specific, a GFP specific or a MYC-specific antibody at 2 dpai. Co-expression of NbBeclin1:eGFP, MYC:NIb, and the empty vector in *N. benthamiana* leaves was used as a negative control. The CBB-stained gel shows sample loadings. G, RT-qPCR detection of TVBMV RNA in the *N. benthamiana* leaves co-expressing NbBeclin1:eGFP and HA:NbRPL1 at 2 dpai. Co-expression of NbBeclin1:eGFP and empty vector in *N. benthamiana* leaves was used as the negative control. Expression of *NbEF1α* was used as an internal control. Error bars indicate the standard deviation of three biological replicates per treatment. Statistical significance was determined using a two-tailed Student's *t* test (*$P < 0.05$). H, Competitive binding of NbRPL1 and NbBeclin1 to NIb in vitro. The mixed protein samples of HIS:MBP:MYC:NIb, HIS:eGFP:NbBeclin1, and HIS:HA:NbRPL1 with different concentrations were adsorbed with GFP-Trap_A beads followed by western blotting detection using a HA specific, a GFP specific or a MYC specific antibody. Band intensities shown in (D), (F), and (H) were quantified with ImageJ software.

silencing of *NbRPL1* expression in *N. benthamiana* inhibited TVBMV infection (Figures 4 and 5). These results indicate that NbRPL1 is a host factor involved in TVBMV infection.

Increasing evidence has shown that ribosomal proteins play active roles in potyvirus infections. For example, TuMV requires both ribosomal protein S6 (RPS6) and RPS6 kinase for its infection in *N. benthamiana* (Rajamäki et al., 2017). PVA protein translation has been shown to be promoted by *A. thaliana* 60S acidic ribosomal protein (Hafrén et al., 2013). Further, silencing ribosomal protein genes *RPL19*, *RPL13*, *RPL7*, or *RPS2* expression inhibited TuMV infection in *N. benthamiana* plants (Yang et al., 2009). Tobacco etch virus protein translation is increased by 80S cytoplasmic ribosomes and 60S ribosomal subunits (Martínez and Daròs, 2014). Most of the reported ribosomal proteins that regulate viral infection are localized in the cytoplasm (Hafrén et al., 2013). Here, we found that the chloroplast ribosomal protein NbRPL1 can interact with TVBMV NIb and enhance TVBMV RNA and NIb accumulation in the 6K2-induced vesicles, but the overexpression of NbRPL1 had little effect on TVBMV protein translation (Figures 1, 3, 4, and 5).

Autophagy plays an antiviral role in plant–virus interactions (Yang et al., 2020). On the other hand, plant viruses can hijack the autophagy pathway to promote their pathogenesis (Yang et al., 2020). A previous study has shown that TuMV NIb interacts with the autophagy receptor NbBeclin1 and is degraded through autophagy-related pathways (Li et al., 2018). In this study, we also determined that NbBeclin1 can interact with TVBMV NIb and induce degradation of TVBMV NIb in a NbRPL1 dose-dependent manner (Figure 6), indicating that NbRPL1 is employed by TVBMV to antagonize autophagy and promote pathogenesis. NbBeclin1 co-localizes with TVBMV VRCs in chloroplasts (Li et al., 2018). Our analyses also revealed that 9.39% and 4.85% of NbRPL1/NIb complexes co-localized with NbBeclin1 in cytoplasm and chloroplasts, respectively (Supplemental Figure S4). Considering the results described above, we postulate that the competition between NbRPL1–NIb and NbBeclin1–NIb interactions occurs in both cytoplasm and chloroplasts.

A recent study has shown that *Phytophthora infestans* effector AVRvnt1 interacts with chloroplast protein glycerate 3-kinase (GLYK) and activates Rpi-vnt1.1-mediated host resistance. A mutant GLYK lacking its cTP domain cannot activate Rpi-vnt1.1-mediated host resistance (Gao et al., 2020). Several plant viral proteins also contain cTPs that can autonomously target chloroplasts. For example, the cTP in the N-terminus of cucumber necrosis virus CP is essential for chloroplast targeting (Hui et al., 2010). The lolium latent virus CP also contains a typical cTP domain and localizes to chloroplasts (Vaira et al., 2018). The cTP domain of tomato yellow leaf curl virus C4 protein plays an important role in translocating C4 protein from plasma membrane to chloroplasts upon activation of host defense mechanisms (Medina-Puche et al., 2020). Plant viruses lacking cTP need to hijack chloroplast factors with cTPs for targeting chloroplasts. Chloroplast protein plastocyanin contains a cTP and has been shown to interact with PVX CP. Silencing of *plastocyanin* expression reduces the accumulation of PVX CP in chloroplasts (Qiao et al., 2009). Chl-PGK has also been shown to be involved in targeting BaMV RNA to chloroplasts in *N. benthamiana* leaves (Cheng et al., 2013). NbcpHsp70-2 interacts with BaMV replicase, and its mislocalization affects BaMV replication (Huang et al., 2017). In our study, we found that the NIb-interacting chloroplast ribosomal protein NbRPL1 contains a cTP domain that is necessary for chloroplast targeting (Figure 2). We also found that during TVBMV infection, the NbRPL1/NIb complex co-localizes with TVBMV VRCs on chloroplasts (Figures 1 and 3). Deletion of cTP from NbRPL1 decreased the chloroplast targeting of the NbRPL1/NIb complex (Figure 2). However, cTP is dispensable for the interaction between NbRPL1 and NIb (Figure 2F).

Based on the above results, we propose a working model for the role of NbRPL1 in TVBMV infection. Upon TVBMV infection, replicase NIb is recognized and then degraded by the NbBeclin1-mediated autophagy. To prevent this degradation, TVBMV recruits NbRPL1, which competes with NbBeclin1 for NIb, to prevent NIb degradation and promote TVBMV infection. NbRPL1 localizes in the VRCs in chloroplasts with the assistance of its cTP. The findings presented here advance our understanding of the roles of chloroplast ribosomal proteins in potyvirus pathogenesis and reveal an antiviral breeding strategy for potyvirus resistance.

Materials and methods

Plant growth

Nicotiana benthamiana seedlings were grown in pots containing isotonic soil matrix (pH 5.8–6.5) inside a growth chamber maintained at 22 ± 2°C, with a 16 h/8 h (light/dark) photoperiod, and 70% relative humidity.

Plasmid construction

Total RNA was isolated from leaf samples harvested from *N. benthamiana* plants using TRIzol reagent. The RNA samples were treated with DNase I, and then used for cDNA synthesis as described previously (Cheng et al., 2020). The full-length chloroplast 50S *ribosomal protein 1* gene (*NbRPL1*; Niben101Scf03253g02006.1) and *elongation factor thermo unstable* gene (*NbEF-Tu*; Niben101Scf03816g02010) were PCR-amplified from *N. benthamiana* cDNA using a High-fidelity Phusion DNA polymerase (Thermo Fisher Scientific, Waltham, MA, USA), and cloned individually into the pEHISeGFP vector to produce pEHIS:eGFP:NbRPL1 and pEHIS:eGFP:NbEF-Tu using a Ligation-Free Cloning System (Applied Biological Materials, Richmond, BC, Canada) following the manufacturer's instructions. The TVBMV NIb-coding sequence (JQ407082) was PCR-amplified from the cDNA from a TVBMV-infected plant, and cloned into pUTRMYC (an expression vector containing a 35S promoter, the 5′-untranslated region of TVBMV, and 2× MYC-coding sequence), pEHISMBPMYC (a vector containing a 35S promoter, and the Histone-, MBP-, and MYC-coding sequences), pCamYN (a vector containing the 5′ half of the

YFP gene), pGBKT7 (binding domain), and pGADT7 (activation domain). The *NbRPL1* sequence was also cloned into pCamYC (a vector containing the 3′ half of the *YFP* gene) and pUTRHA (an expression vector containing a 35S promoter, the 5′-untranslated region of TVBMV, and the HA-coding sequence). Expression vectors pUTRMYC, pUTRHA, pEHISMBPMYC, and pEHISMBP were constructed previously in our laboratory. Full-length *N. benthamiana Beclin1* (*NbBeclin1*; AY701316.1) was PCR-amplified, and cloned into the pCamYC, pGADT7, and pGBKT7 vectors. In addition, the full-length *NbRPL1* and its deletion mutants (i.e. NbRPL1$^{\Delta cTP(N61aa)}$, NbRPL1$^{\Delta N41aa}$, NbRPL1$^{\Delta N20aa}$, NbRPL1$^{\Delta N42-61aa}$:DsRed, NbRPL1$^{\Delta N21-61aa}$:DsRed, NbRPL1$^{\Delta N21-41aa}$:DsRed, NbRPL1$^{1-280aa}$, and NbRPL1$^{281-340aa}$) were inserted individually into the XbaI/BamHI site in the pCameGFP and pCamDsRed vectors. For VIGS assays, a fragment representing a partial sequence of the *NbRPL1* gene (nucleotides 553–1002) was PCR-amplified, and inserted individually into a TRV-based VIGS vector (Liu et al., 2002) to produce pTRV2-NbRPL1. *RLUC* was inserted between the *NIb* and *CP* gene in the pCB301TVBMV$^{\Delta GDD}$ vector (a vector expressing a replication-deficient mutant of TVBMV; Supplemental Figure S2) to produce pCB301TVBMV$^{\Delta GDD}$-RLUC. Further, a 35S-FLUC-NOS sequence was cloned into the pCB301TVBMV$^{\Delta GDD}$-RLUC vector to produce pCB301TVBMV$^{\Delta GDD}$-RLUC//FLUC (Supplementary Figure S2). Primers used in this study are listed in Supplemental Table S1.

Virus inoculation and transient gene expression

Plasmids pCamTVBMV-GFP, pCamTVBMV$^{\Delta P3NPIPO}$-GFP, pTRV1, pTRV2, pCB301TVBMV$^{\Delta GDD}$-RLUC//FLUC, and various transient expression vectors were individually transformed into *Agrobacterium tumefaciens* strain GV3101. The transformed *A. tumefaciens* cell cultures were maintained as described previously (Cheng et al., 2020). After incubation in an induction buffer containing 10-mM MES (pH 5.6), 10-mM $MgCl_2$, and 200-μM acetosyringone, the cell cultures were pelleted individually, and then diluted to OD_{600} = 0.5 for virus inoculations, or to OD_{600} = 0.2 for transient expression and BiFC assays in 4-week-old *N. benthamiana* plants through agroinfiltration using 1-mL needleless syringes.

In vitro pull-down and in vivo Co-IP assays

Escherichia coli cells (Rossetta, DE3) transformed with pEHIS:eGFP, pEHIS:eGFP:NbRPL1, pEHIS:eGFP:NbEF-Tu, or pEHIS:MBP:MYC:NIb were grown on an orbital shaker (220 rpm) at 28°C until an OD_{600} of 0.5 was attained. After the addition of IPTG (0.4 mM for the pEHIS:eGFP-transformed cells or 2 mM for the pEHIS:MBP-transformed cells), the cultures were incubated again on the shaker for 12 h at 16°C. The resulting cultures were pelleted by centrifugation at 8,000 rpm, resuspended separately in 20-mL lysis buffer (0.3 M NaCl, 10-mM imidazole, 1-mM DTT, 0.25-mM PMSF, and 0.5 mg·mL^{-1} lysozyme in PBS [pH 7.4]), and incubated for 30 min at 37°C. The cells were disrupted by sonication on ice, and pelleted by centrifugation for 10 min at 8,000 rpm at 4°C. The supernatant of each sample was collected into a new centrifuge tube, and centrifuged for 20 min at 8,000 rpm at 4°C. The resulting supernatant was collected again after filtering through a 0.22 μm filter. Recombinant proteins in each filtered supernatant were purified using a high-affinity Ni-charged resin (GenScript, New Jersey, USA), and the captured proteins were dialyzed overnight in a dialysis buffer (0.3 M NaCl, 1 M Tris-HCl [pH 7.5], and 1-mM DTT in PBS [pH 7.4]) at 4°C. Twenty micrograms of purified HIS:eGFP:NbRPL1 or HIS:GFP:NbEF-Tu was added to a 1.5-mL centrifuge tube followed by the addition of 20-μg HIS:MBP:MYC:NIb, 500-μL dilution buffer (pH 7.4), and 20-μL GFP-Trap_A beads (Chromotek, Munich, Germany). The centrifuge tubes were incubated for 2 h on ice on an orbital shaker. The beads were rinsed 10 times with PBS (pH 7.4), and then resuspended in 1× SDS-sample buffer. After 10 min boiling and then 10 min incubation on ice, the proteins were separated by SDS–PAGE, and subsequently transferred onto nitrocellulose membranes. The membranes were probed with an MYC-specific antibody (Abways Technology, Shanghai, China). In vivo Co-IP assays were performed using a method reported previously (Geng et al., 2017). Western blotting assay was conducted as described previously (Cheng et al., 2020).

Y2H assay

The Y2H assay was performed according to the manufacturer's instructions (Clontech, Mountain View, CA, USA). Briefly, yeast cell strain Y2H Gold was transformed with various expression constructs and then grown on a selection medium (SD/-Trp/-Leu) for 3 d. The selected colonies were then grown on a highly stringent selection medium supplemented with X-α-Gal (e.g. SD/-Trp/-Leu/-His/-Ade/ + X-α-Gal) for 4 d.

Subcellular localization and BiFC assays

Subcellular localization and BiFC assays were performed using *N. benthamiana* leaves. Fluorescence from GFP, YFP, or DsRed in leaf cells was examined and imaged at 36 hpai under a Zeiss LSM800 laser scanning confocal microscope (Leica Microsystems, Wetzlar, Germany). The excitation wavelength for GFP was set at 488 nm (argon ion laser) and the emission was captured at 505–545 nm. The excitation wavelength for YFP was set at 514 nm (argon ion laser) and the emission was captured at 560–585 nm. The excitation wavelength for DsRed was set at 543 nm and the emission was captured at 590–620 nm. Autofluorescence from chloroplasts was captured at 675–720 nm. Confocal images were created using a pinhole size of 1 AU with gains of 680, maximum light intensity value for the samples expressing YFP and eGFP, and 20% of maximum light intensity value for the samples expressing DsRed, mCherry, and autofluorescence from chloroplasts. The captured images were further processed using the Zeiss LSM Image Examiner version 4.0 or ZEN blue version 2.1 software (Leica Microsystems, Wetzlar, Germany).

VIGS

Plasmids pTRV2-NbRPL1, pTRV2-GUS, and pTRV1 were individually transformed into *A. tumefaciens* strain GV3101 cells. After propagation and incubation, each *A. tumefaciens* culture was pelleted and diluted to OD_{600} of 0.5. The *A. tumefaciens* culture harboring pTRV1 was mixed with the *A. tumefaciens* culture harboring pTRV2-NbRPL1 (the virus is referred to as TRV-NbRPL1) or pTRV2-GUS (referred to as TRV-GUS) at a ratio of 1:1 (v/v). The mixed cultures were separately infiltrated into the leaves of *N. benthamiana* plants. At 7 dpai, the leaves above the infiltrated leaves of the assayed plants were further infiltrated with an *A. tumefaciens* culture (OD_{600} = 0.5) carrying pCamTVBMV-GFP or pCamTVBMV$^{\Delta P3NPIPO}$-GFP.

RT-qPCR

Primers used in RT-qPCR were designed using an online tool (http://www.oligoarchitect.com/SYBRGreenSearchServlet), and are listed in Supplemental Table S1. Total RNA was extracted from leaf samples using TRIzol reagent. Reverse transcription (10 μL each) was conducted using 2 μL of 5× HiScript II qRT Super Mix II reagent (Vazyme, Nanjing, China) and 500 ng total RNA. Quantitative PCR reactions (20 μL each) were conducted using 10 μL 2× ChamQ SYBR qPCR Master Mix reagent (Vazyme, Nanjing, China), 10 μM forward primer, 10 μM reverse primer, and 1-μL diluted cDNA on a LightCycler 96 machine (Roche, Basel, Switzerland). Relative gene expression was calculated using the $2^{-\Delta\Delta Ct}$ method as described previously (Livak and Schmittgen, 2001). *NbEF1α* expression was used as an internal control. All experiments were repeated three times.

Protoplast preparations

Protoplast isolation from 4-week-old *N. benthamiana* plant leaves and their transfections were performed as described previously (Schweiger and Schwenkert, 2014). After transfection, protoplasts were incubated at 26°C for 12 h and extracted for total RNA prior to RT-qPCR.

Dual-luciferase activity assay

Agrobacterium tumefaciens cells carrying pCB301TVBMV$^{\Delta GDD}$-RLUC//FLUC (Supplemental Figure S3) were cultured, pelleted, induced, and then diluted to OD_{600} = 0.05. The diluted cell suspension was infiltrated into leaves of the NbRPL1-overexpressing or control *N. benthamiana* plants to determine the effect of *NbRPL1*-silencing on virus accumulation. At 60 hpai, leaf discs (1 cm in diameter each) were collected from the infiltrated leaves and placed inside 2.0-mL centrifuge tubes. Each centrifuge tube was added with 150-μL lysis buffer (Vazyme, Nanjing, China), vortexed for 15 min, and then centrifuged for 2 min at 12,000 rpm. The resulting supernatant was collected from each tube and was used for luciferase activity assays using the Dual-Luciferase Reporter Assay Kit (Vazyme, Nanjing, China). The experiment was repeated three times.

Statistical analyses

The data shown in this study are means of three independent experiments. When two sets of data are compared, they were analyzed by the Student's *t* test. The $P < 0.05$ are indicated as asterisks, and the $P < 0.01$ are indicated as double asterisks. ImageJ software was used to quantify the intensity of the bands in Western blotting.

Accession numbers

The sequences of *NbRPL1* (accession number: Niben101Scf03253g02006.1), *NbEF-Tu* (accession number: Niben101Scf03816g02010.1), and *NbBeclin1* (accession number: AY701316.1) can be found in the SOL Genomics Network (SGN, https://solgenomics.net/) and NCBI.

Supplemental data

The following materials are available in the online version of this article.

Supplemental Figure S1. Peptides of NbRPL1 and NbEF-Tu identified through liquid chromatography tandem mass spectrometry.

Supplemental Figure S2. A schematic diagram of plasmid pCB301TVBMV$^{\Delta GDD}$-RLUC//FLUC.

Supplemental Figure S3. Relative expression of autophagy-associated genes.

Supplemental Figure S4. Co-localization of the NIb/NbRPL1 complex with NbBeclin1.

Supplemental Table S1. Primers used in this study.

Funding

This work was supported by funds from the National Natural Science Foundation of China (NSFC; grant nos. 32072387, 31720103912, 31871933), "Taishan Scholar" Construction Project (grant no. TS201712023), and Shandong "Double Tops" Program (grant no. SYL2017XTTD11).

Conflict of interest statement. The Authors declare that there is no conflict of interest.

References

Bhat S, Folimonova SY, Cole AB, Ballard KD, Lei Z, Watson BS, Sumner LW, Nelson RS (2013) Influence of host chloroplast proteins on *Tobacco mosaic virus* accumulation and intercellular movement. Plant Physiol **161**: 134–147

Bhattacharyya D, Chakraborty S (2018) Chloroplast: the Trojan horse in plant-virus interaction. Mol Plant Pathol **19**: 504–518

Bhattacharyya D, Gnanasekaran P, Kumar RK, Kushwaha NK, Sharma VK, Yusuf MA, Chakraborty S (2015) A geminivirus betasatellite damages the structural and functional integrity of chloroplasts leading to symptom formation and inhibition of photosynthesis. J Exp Bot **66**: 5881–5895

Bionda T, Tillmann B, Simm S, Beilstein K, Ruprecht M, Schleiff E (2010) Chloroplast import signals: the length requirement for translocation *in vitro* and *in vivo*. J Mol Biol **402**: 510–523

Cheng DJ, Tian YP, Geng C, Guo Y, Jia MA, Li XD (2020) Development and application of a full-length infectious clone of potato virus Y isolate belonging to SYR-I strain. Virus Res **276**: 197827

Cheng SF, Huang YP, Chen LH, Hsu YH, Tsai CH (2013) Chloroplast phosphoglycerate kinase is involved in the targeting of

Bamboo mosaic virus to chloroplasts in *Nicotiana benthamiana* plants. Plant Physiol **163**: 1598–1608

Chung BY-W, Miller WA, Atkins JF, Firth AE (2008) An overlapping essential gene in the Potyviridae. Proc Natl Acad Sci U S A **105**: 5897–5902

Emanuelsson O, Nielsen H, heijne Gv (1999) ChloroP, a neural network-based method for predicting chloroplast transit peptides and their cleavage sites. Protein Sci **8**: 978–984

Gao C, Xu H, Huang J, Sun B, Zhang F, Savage Z, Duggan C, Yan T, Wu CH, Wang Y, et al. (2020) Pathogen manipulation of chloroplast function triggers a light-dependent immune recognition. Proc Natl Acad Sci U S A **117**: 9613–9620

Geng C, Wang HY, Liu J, Yan ZY, Tian YP, Yuan XF, Gao R, Li XD (2017) Transcriptomic changes in *Nicotiana benthamiana* plants inoculated with the wild-type or an attenuated mutant of *Tobacco vein banding mosaic virus*. Mol Plant Pathol **18**: 1175–1188

Geng C, Yan ZY, Cheng DJ, Liu J, Tian YP, Zhu CX, Wang HY, Li XD (2017) *Tobacco vein banding mosaic virus* 6K2 protein hijacks NbPsbO1 for virus replication. Sci Rep **7**: 43455

Hafrén A, Eskelin K, Mäkinen K (2013) Ribosomal protein P0 promotes *Potato virus A* infection and functions in viral translation together with VPg and eIF(iso)4E. J Virol **87**: 4302–4312

Huang YW, Hu CC, Tsai CH, Lin NS, Hsu YH (2017) Chloroplast Hsp70 isoform is required for age-dependent tissue preference of *Bamboo mosaic virus* in mature *Nicotiana benthamiana* leaves. Mol Plant Microbe Interact **30**: 631–645

Hui E, Xiang Y, Rochon D (2010) Distinct regions at the N-terminus of the *Cucumber necrosis virus* coat protein target chloroplasts and mitochondria. Virus Res **153**: 8–19

Ivanov KI, Eskelin K, Lõhmus A, Mäkinen K (2014) Molecular and cellular mechanisms underlying potyvirus infection. J Gen Virol **95**: 1415–1429

Kaido M, Abe K, Mine A, Hyodo K, Taniguchi T, Taniguchi H, Mise K, Okuno T (2014) GAPDH-A a recruits a plant virus movement protein to cortical virus replication complexes to facilitate viral cell-to-cell movement. PLoS Path **10**: e1004505

Koonin EV (1991) The phylogeny of RNA-dependent RNA polymerases of positive-strand RNA viruses. J Gen Virol **72**: 2197–2206

Li F, Zhang C, Li Y, Wu G, Hou X, Zhou X, Wang A (2018) Beclin1 restricts RNA virus infection in plants through suppression and degradation of the viral polymerase. Nat Commun **9**: 1268

Li Y, Cui H, Cui X, Wang A (2016) The altered photosynthetic machinery during compatible virus infection. Curr Opin Virol **17**: 19–24

Liu Y, Schiff M, Marathe R, Dinesh-Kumar SP (2002) Tobacco *Rar1*, *EDS1* and *NPR1/NIM1* like genes are required for *N*-mediated resistance to tobacco mosaic virus. Plant J **30**: 415–429

Livak KJ, Schmittgen TD (2001) Analysis of relative gene expression data using real-time quantitative PCR and the $2^{-\Delta\Delta CT}$ method. Methods **25**: 402–408

Martínez F, Daròs J-A (2014) *Tobacco etch virus* protein P1 traffics to the nucleolus and associates with the host 60S ribosomal subunits during infection. J Virol **88**: 10725–10737

Medina-Puche L, Tan H, Dogra V, Wu M, Rosas-Diaz T, Wang L, Ding X, Zhang D, Fu X, Kim C, et al. (2020) A defense pathway linking plasma membrane and chloroplasts and co-opted by pathogens. Cell **182**: 1109–1124

Montasser MS, Al-Own FD, Haneif AM, Afzal M (2012) Effect of *Tomato yellow leaf curl bigeminivirus* (TYLCV) infection on tomato cell ultrastructure and physiology. Can J Plant Pathol **34**: 114–125

Qiao Y, Li HF, Wong SM, Fan ZF (2009) Plastocyanin transit peptide interacts with *Potato virus X* coat protein, while silencing of plastocyanin reduces coat protein accumulation in chloroplasts and symptom severity in host plants. Mol Plant Microbe Interact **22**: 1523–1534

Rajamäki M-L, Xi D, Sikorskaite-Gudziuniene S, Valkonen JPT, Whitham SA (2017) Differential requirement of the ribosomal protein S6 and ribosomal protein S6 kinase for plant-virus accumulation and interaction of S6 kinase with potyviral VPg. Mol Plant-Microbe Interact **30**: 374–384

Revers F, García JA (2015) Molecular biology of potyviruses. Adv Virus Res **92**: 101–199

Schweiger R, Schwenkert S (2014) Protein-protein interactions visualized by bimolecular fluorescence complementation in tobacco protoplasts and leaves. J Vis Exp **85**: e51327

Shi B, Lin L, Wang S, Guo Q, Zhou H, Rong L, Li J, Peng J, Lu Y, Zheng H, et al. (2016) Identification and regulation of host genes related to *Rice stripe virus* symptom production. New Phytol **209**: 1106–1119

Vaira AM, Lim HS, Bauchan G, Gulbronson CJ, Miozzi L, Vinals N, Natilla A, Hammond J (2018) The interaction of Lolium latent virus major coat protein with ankyrin repeat protein NbANKr redirects it to chloroplasts and modulates virus infection. J Gen Virol **99**: 730–742

Wei T, Huang T-S, McNeil J, Laliberté J-F, Hong J, Nelson RS, Wang A (2010) Sequential recruitment of the endoplasmic reticulum and chloroplasts for plant potyvirus replication. J Virol **84**: 799–809

Wei T, Zhang C, Hou X, Sanfaçon H, Wang A (2013) The SNARE protein Syp71 is essential for turnip mosaic virus infection by mediating fusion of virus-induced vesicles with chloroplasts. PLoS Path **9**: e1003378

Yang C, Zhang C, Dittman JD, Whitham SA (2009) Differential requirement of ribosomal protein S6 by plant RNA viruses with different translation initiation strategies. Virology **390**: 163–173

Yang M, Ismayil A, Liu Y (2020) Autophagy in plant-virus interactions. Annu Rev Virol **7**: 403–419

Zhang T, Liu P, Zhong K, Zhang F, Xu M, He L, Jin P, Chen J, Yang J (2019) Wheat yellow mosaic virus NIb interacting with host light induced protein (LIP) facilitates its infection through perturbing the abscisic acid pathway in wheat. Biology **8**: 80

Zhao J, Liu Q, Zhang H, Jia Q, Hong Y, Liu Y (2013) The rubisco small subunit is involved in tobamovirus movement and *Tm-22*-mediated extreme resistance. Plant Physiol **161**: 374–383

Zhao J, Zhang X, Hong Y, Liu Y (2016) Chloroplast in plant-virus interaction. Front Microbiol **7**: 1565